

Relation between spin–orbit induced spin polarization, Fano-effect and circular dichroism in soft x-ray photoemission

Dmitry Vasilyev[✉], Katerina Medjanik, Sergey Babenkov, Martin Ellguth, Gerd Schönhense and Hans-Joachim Elmers

Institut für Physik, Johannes-Gutenberg-Universität, Staudingerweg 7, 55128 Mainz, Germany

E-mail: dmvasily@uni-mainz.de

Received 2 July 2019, revised 1 November 2019

Accepted for publication 3 December 2019

Published 31 December 2019



Abstract

A Feynman diagram analysis of photoemission probabilities suggests a relation between two final-state spin polarization effects, the optical spin-orientation originating from the interaction with circularly polarized light (P_{OO} , Fano effect) and the spin polarization induced by the spin–orbit scattering (P_{\perp} , Mott effect). The analysis predicts that P_{\perp} is proportional to the product of P_{OO} and the circular dichroism in the angular distribution (CDAD) of photoelectrons. To confirm this prediction, the spin polarization of photoelectrons excited by soft x-ray radiation from initial spin-degenerate bulk states of tungsten using time-of-flight momentum microscopy with parallel spin detection has been measured. By measurement of four independent photoemission intensities for two opposite spin directions and opposite photon helicity, CDAD, Fano, and Mott effect are distinguished. The results confirm the prediction from the Feynman diagram analysis.

Keywords: spin-resolved momentum microscopy, electronic structure, spin-polarization of bulk bands

(Some figures may appear in colour only in the online journal)

Introduction

Spin-resolved photoelectron spectroscopy has a long tradition, see e.g. textbooks for work in the gas phase [1] and for solids [2, 3]. After pioneering work at ETH Zurich on spin polarized electrons from ferromagnetic materials [4] and optical spin orientation in GaAs [5], angular-resolved photoelectron spectroscopy (ARPES) with spin-resolution developed rapidly and became a powerful tool for analyzing exchange-split bands in ferromagnets [6]. The method was also used for symmetry-resolved band mapping of non-magnetic metals [7] and adsorbates [8]. In the last decade, spin-ARPES activities were strongly intensified by the discovery of topological materials with special spin textures [9–11].

In the x-ray range only a few spin-resolved core level measurements at ferromagnets have been performed using lab sources [12–14] and hard x-rays [15, 16]. In the valence range two angle-integrating measurements have been published [17, 18];

in both experiments the spin signal was close to the detection limit. The low photoemission cross sections in the x-ray range so far were prohibitive for k -resolved spin measurements. On the other hand, angle-resolving [19] and k -resolving [20] spectroscopy have revealed the power of x-ray ARPES to study the electronic structure deep in the bulk of a material, excluding surface effects. As the bulk density of states and the Fermi surface are responsible for practically all transport and thermodynamic phenomena, detailed information on the true bulk electronic structure is mandatory for basic materials research and materials tailoring. It would be highly desirable to include the spin degree of freedom in the information content of bulk-sensitive photoemission.

Previous measurements at low energies have demonstrated that multichannel spin detection using imaging spin filters [21, 22] can increase the effective figure-of-merit by orders of magnitude. In the present work this technique was implemented in a momentum-resolving photoelectron spectrometer,

thus overcoming the count-rate limitation of x-ray ARPES. Since the studied spin-polarization is mediated by spin-orbit interaction, we have chosen to study the bulk bands of tungsten ($Z = 76$).

Several mechanisms may give rise to photoelectron spin polarization; we distinguish between initial-state, final-state and matrix-element effects. Examples for materials with initial-state spin polarization are ferromagnets with exchange-split bands or the special (ground-state) spin texture induced by the Rashba effect. Corresponding asymmetries have been discussed in [23]. Both are excluded for tungsten bulk bands; the time-reversal invariant surface state with Dirac-like spin texture [24] is not visible at the photon energies used [20].

The ‘final-state effect’ was first described by Kirschner *et al* [25]. Initially unpolarized electrons excited into the upper Bloch states may acquire spin polarization when crossing the surface. The crystal surface separates the Bloch-spinor regime from the free-electron spinor regime, in which the detector is placed. Matching these relativistic wave functions at the boundary then may lead to a net spin polarization of the transmitted electrons, if significant spin-orbit interaction is present at the surface. In the present experiment we can rule out a significant contribution of this effect, because the kinetic energy of the photoelectrons is too high.

The matrix-element-induced spin polarization depends on the photon polarization (since the matrix element itself depends on photon polarization). The best-studied case is the optical spin orientation by circularly polarized light (also termed Fano effect), which was initially predicted for photoemission from Cs atoms [26]. This phenomenon is exploited in the generation of spin-polarized electrons in GaAs [5]. The selection rules for circularly polarized light ($\Delta m_j = \pm 1$) lead to a population of final-state partial waves with a preferential spin orientation pointing along the photon spin s_γ . We term the resulting spin component along the photon spin the *Fano component*.

The matrix element gives rise to a second spin component that is oriented perpendicular to the plane spanned by the surface normal and the momentum of the outgoing electron. Heinzmann and Dil [27] give a detailed discussion on the nature of this component, originating from a phase-shift difference between interfering final-state partial waves. We adopt the notation P_\perp for this perpendicular component from [27] and earlier gas-phase work with unpolarized [28] and linearly-polarized light [29]. Discussing photoemission with circularly-polarized light, the quantity of circular dichroism in the angular distribution (CDAD) must be addressed. In the context of topological systems CDAD is sometimes considered as a substitute for spin-resolved measurements. On the other hand, CDAD for nonmagnetic systems can be explained in a non-relativistic model (for details, see [30]). It is the general understanding that CDAD and the Fano effect have nothing in common.

In this article, a previously overseen relation between the non-relativistic CDAD, and the two relativistic quantities of the Fano effect, P_{OO} , and the perpendicular spin polarization component, P_\perp , has been derived using a Feynman-diagram

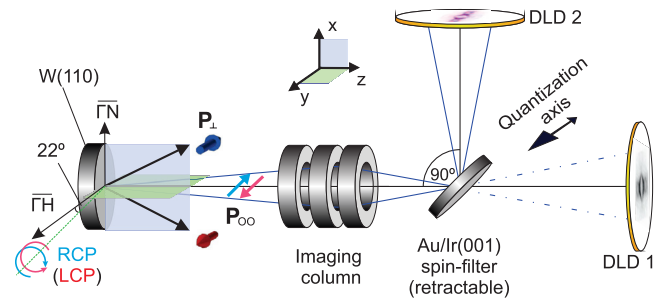


Figure 1. Sketch of the experiment illustrating the symmetry properties of the spin polarization. Optical spin orientation by the right- (left-) circularly polarized photon beam (RCP, LCP) induces the ‘Fano-component’ $P_{OO,RCP(LCP)}$ pointing along the photon spin. In addition, the transversal spin component P_\perp occurs due to interference of final-state partial waves. P_\perp vanishes in the plane of incidence, whereas there is no such restriction for P_{OO} .

description of probabilities. Using four independent measurements (two opposite photon helicities and two opposite spin quantization directions), the prediction of the Feynman-diagram analysis has been confirmed. We experimentally demonstrate a non-vanishing spin-polarization of photoelectrons excited by soft x-rays from initial bulk states of a non-magnetic centrosymmetric material by the example of the bcc metal W. Exploiting the circular polarization of the incident light beam, the (E_B, k) texture of the perpendicular spin component (P_\perp), the Fano-type spin component (P_{OO}) and the circular dichroism (A_{CDAD}), has been measured separately. The predicted relation of spin polarization effects and polarization-dependent dichroic effects is validated by the example of electronic bulk bands of tungsten.

Methods

The photoemission experiments were performed at beamline P04 of the PETRA III storage ring (DESY, Hamburg), providing almost completely ($>95\%$) circularly polarized light in the soft x-ray regime. Here we show data taken at a photon energy of 447 eV and an incidence angle of 22° with respect to the surface plane that we assume as grazing incidence in the following. The geometry of the setup is sketched in figure 1. The plane of photon incidence is the yz -plane, which coincides with the $\bar{\Gamma}$ - \bar{H} azimuth of the crystal surface. For the detection of photoelectrons time-of-flight (ToF) momentum microscopy with imaging spin filter was used; for details, see [31, 32]. The method allows detecting the photoemission intensity $I(E_B, k_x, k_y)$ as a function of momentum components k_x and k_y (parallel to the sample surface), and binding energy E_B .

Spin-resolution along the y -axis is achieved by combining full-field k -imaging and ToF energy recording with an imaging spin filter, in our case a pseudomorphic Au monolayer on Ir (001) [33]. This surface was chosen due to the high spin-sensitivity (70%) and incredibly long lifetime (more than 12 months in ultra-high vacuum). We performed measurements at the two scattering energies of 10.25 eV and 11.50 eV with opposite scattering asymmetry.

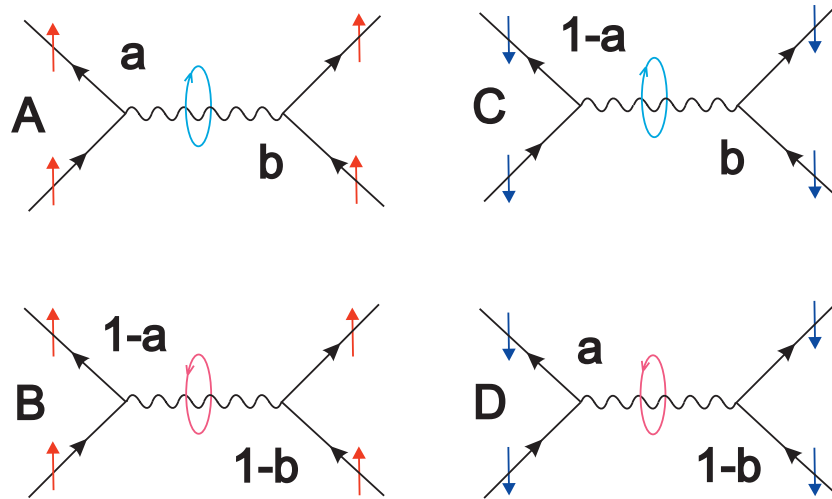


Figure 2. The Feynman diagrams A–D describe the scattering probabilities for spin up/down and circular right/left virtual photons. Red (blue) arrows designate spin-up (spin-down) states. a and b denote the probabilities of the different branches (see text).

Results and discussion

Considering initial and final states that are spin-degenerate, the occurrence of a finite photoelectron spin polarization as predicted in [23] by *ab initio* methods appears surprising at first sight. For an explanation, we propose the following model based on electron scattering described by Feynman diagrams [34, 35] as shown in figure 2. The Feynman diagram describes an electron scattering event in two steps proceeding along the horizontal time axis and the vertical space axis. In the first step, the incident electron occupies an unoccupied state. This is considered as an annihilation of an electron and a hole state. Because the hole state represents an antiparticle, it moves backward in time and space, i.e. it is depicted as an outgoing arrow. The annihilation of hole and electron creates a photon. In the second step, the photon annihilates and creates a particle-antiparticle pair. The antiparticle (hole) moves again backward in time and space and is now depicted as an incoming arrow. The electron represented by the outgoing arrow is then detected.

The spin state does not change in a photon-electron interaction process. However, different scattering probabilities may lead to a finite spin-polarization [23]. Each scattering path comprises two events that contribute to the total probability of this path. In the first step, the scattering process creates a virtual photon, which is either left or right circularly polarized. This process may be described as an *inverse Fano effect* because it represents the reverse process of a circularly polarized photon creating a spin-polarized photoelectron, known as the Fano effect. Experimentally a very similar *inverse Fano process* has already been introduced by Eminyan and Lampel [36]. This *inverse Fano process* is mediated by spin-orbit coupling and therefore spin-dependent. We denote the probability a for creating a RCP photon in the scattering process of a spin-up electron (see figure 2 case A, red arrows). Consequently, the probability to create an LCP photon is $1 - a$ (see figure 2 case B). The analogue scattering process for a spin-down electron has opposite probabilities, $1 - a$ for creating RCP (see figure 2 case C, blue arrows) and a for LCP photon (see

figure 2 case D). A second step annihilates the virtual photon. The annihilation of a RCP photon scatters a spin-up or spin down electron with a probability b , and an LCP photon scatters an electron with probability $1 - b$. Please note, that the virtual photon annihilation processes are spin-independent because they represent the non-relativistic CDAD effect.

The total probability for a scattering path results from the product of the two events. Summing up the probabilities p^\uparrow for spin-up (figures 2 A and B), i.e. $ab + (1 - a)(1 - b)$, and p^\downarrow for spin-down (figures 2 C and D), i.e. $(1 - a)b + a(1 - b)$, electron scattering and calculating the asymmetry, we derive the perpendicular spin polarization component $P_\perp = (1 - 2a)(1 - 2b)$. The first factor represents the asymmetry of the *inverse Fano process*, $P_{OO} = (1 - 2a)$. Neglecting the definition of the absolute sign and value, we may safely assume that P_{OO} is proportional to the Fano effect itself. The second factor directly describes the CDAD asymmetry $A_{CDAD} = (1 - 2b)$. Consequently, we conclude that the perpendicular spin polarization component is proportional to the product of two asymmetries:

$$P_\perp \propto P_{OO} A_{CDAD}. \quad (1)$$

This equation constitutes a previously overlooked relation between two relativistic spin quantities and the non-relativistic CDAD that can be discussed neglecting the spin and occurs even for light elements [37].

The general idea expressed by the Feynman graphs and resulting equation (1) can be validated for free atoms and molecules recalling the analytical expressions of the quantities, here for a $p_{1/2}$ state. The perpendicular spin component is proportional to $\xi \cos \theta$ (equation (1) in [38]) where θ is the emission angle with respect to the normal. For an initial $p_{1/2}$ state, the parameter ξ is proportional to two matrix elements $|R_S|$ and $|R_D|$ and to the sine of the phase difference $\delta_s - \delta_d$, indicating that it is the result of partial wave interference (equation (5) in [38]). Second, the CDAD asymmetry is proportional to $|R_S||R_D| \sin(\delta_s - \delta_d) \sin \varphi$ [37], whereby in our case, we have $\varphi = \pi/2$. Third, the Fano parameter (equation (4) in [39]) is a constant for the case of an initial $p_{1/2}$ state. To summarize, for

the atomic case of a $p_{1/2}$ state, the perpendicular spin component P_{\perp} is proportional to $P_{OO} \times A_{CDAD}$. A similar consideration also holds for an initial $p_{3/2}$. Thus, for the case of atomic photoemission one can show that the relation denoted in equation (1) is exact. For this particular case, the relation indicates the equivalence of CDAD and spin-polarization measurements for Dirac states [40].

In order to prove this relation, we perform photoemission spectroscopy in the soft x-ray regime, exciting photoelectrons from initial bulk states of tungsten. Tungsten possesses a centrosymmetric crystal lattice and has no spontaneous magnetic order. Therefore, the bulk states of tungsten, i.e. initial and final states of the photoemission process, are spin degenerate.

By scanning the initial photon energy, we obtain the dispersion of electronic states along the perpendicular momentum component k_z assuming the free-electron final state model. We measured spin-integrated intensities for 19 different photon energies in the range from 357 eV to 574 eV, covering one full Brillouin zone. The Fermi surface is the boundary of the occupied part of the valence band states. Momentum sections corresponding to the Fermi energy at different k_z are concatenated to form the Fermi surface in the 3-dimensional momentum space [20]. Figure 3(a) shows the energy isosurface at E_F (i.e. the Fermi surface) and the Brillouin zone (BZ) with marked high symmetry points. The intensity distribution confirms that the initial states are bulk states of tungsten, because surface states do not show dispersion along k_z . It furthermore confirms the assumption that the final states are free-electron like states.

For the spin-resolved measurements, we focus on a photon energy of 447 eV, corresponding to $k_z = 3.9 \times G_{110}$, where G_{110} is the reciprocal lattice vector along the (1 1 0) z -direction. The constant energy maps shown in figures 3(b) and (c) thus represent spherical cuts through the Fermi surface at constant absolute momentum given by the kinetic energy of the final state. The cut is close to the high symmetry Γ -N-H plane of the Fermi surface. We measure four photoelectron intensities, $I_{h,l}^{+,-}$, where the upper index corresponds to the light helicity ‘+’ for RCP light and ‘-’ for LCP light) and the lower index corresponds to the spin detector scattering energy (h—high energy point 11.50 eV and l at low energy point 10.25 eV). Figures 3(b) and (c) depicts the corresponding results for RCP light.

In a first step, we separately evaluate the spin polarization distribution of photoemitted electrons for fixed light helicity, to test the existence of a finite spin polarization. The corresponding polarization values are calculated by

$$P^+ = \frac{I_h^+ - I_l^+}{I_h^+ + I_l^+} \cdot \frac{1}{S}; \quad P^- = \frac{I_h^- - I_l^-}{I_h^- + I_l^-} \cdot \frac{1}{S} \quad (2)$$

where $S =$ is a Sherman function of the spin-filter.

Figures 3(d) and (e) show the spin polarization textures for RCP and LCP light. Note the three-color code: red and blue denote opposite spin directions and the grey value the unpolarized contribution. The spin polarization values for each pixel have been averaged with a Gaussian weight function comprising a radius of 0.1 \AA^{-1} , decreasing the statistical error

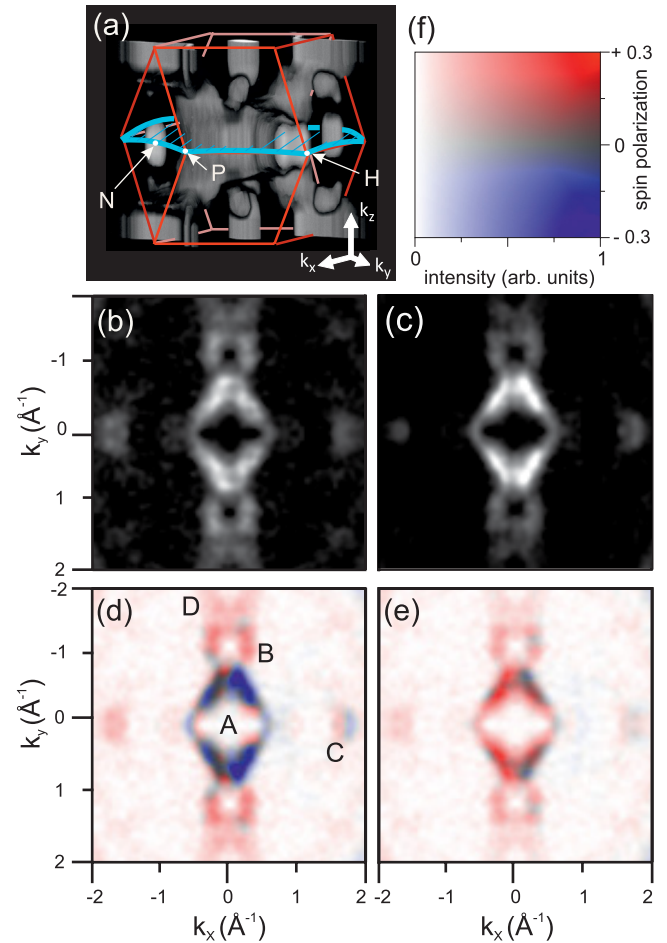


Figure 3. (a) measured 3D Fermi surface, high-symmetry points in the BZ are marked. The blue line marks the spherical section defined by the constant absolute momentum value for which the spin measurement has been performed. (b) Constant energy map of the intensity at the Fermi surface, measured for RCP light after reflection at the spin filter crystal at the high energy point 11.50 eV with positive Sherman function. (c) Corresponding data after reflection at the low energy point 10.25 eV with negative Sherman function. (d) Spin-polarization distribution for RCP light, as determined from the data shown in (b) and (c) and represented in the color code shown in (f). (e) Same for LCP light. (f) Color code for the representation of spin polarization and intensity. Red and blue denote opposite spin directions and the grey value the spin integrated intensity.

for spin polarization values to below 1% near the maximum intensities on the expense of limiting the momentum resolution to 0.2 \AA^{-1} . One can clearly see a non-vanishing spin polarization at the bulk states crossing the Fermi surface for both light helicities. The bulk states with sizable spin polarization correspond to the central octahedron (A) and two of the adjacent balls (B) of the Fermi surface cut close to the Γ -N-H plane (figure 3(a)). The bulk states of the hole-like octahedron centered at the H-points shows almost no spin polarization. The result thus directly proves the existence of spin polarization of emitted electrons from spin-degenerate initial bulk states. The results for opposite helicity differ from each other. In the following, we disentangle the spin polarization contributions from final-state interference and optical orientation.

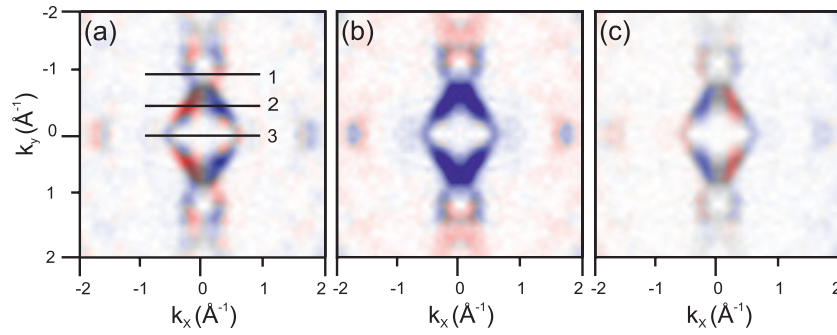


Figure 4. Spin components and circular dichroism. (a) Perpendicular component P_{\perp} . (b) Fano component P_{OO} . (c) CDAD asymmetry A_{CDAD} .

For separating distinct contributions to the observed spin polarization, we consider the measured reflectivity $R_{h,l}$ and the Sherman function $S_l = -S_h = S = 0.7$ in order to obtain the four intensities

$$I_{\text{up,down}}^{+,-} = I_{h,l}^{+,-} / R_{h,l} S. \quad (3)$$

Up (down) refers to the photocurrent for electrons with spin up (down) referring to the spin-quantization axis (y). Using the 4 measured arrays we determine the four quantities of interest (total intensity, P_{\perp} , P_{OO} and A_{CDAD}).

- (i) The total spin-integrated intensity

$$I_0 = I_{\text{up}}^+ + I_{\text{down}}^+ + I_{\text{up}}^- + I_{\text{down}}^- \quad (4)$$

serves as the normalization quantity in order to obtain the polarization or asymmetry values.

- (ii) The perpendicular spin polarization (figure 4(a))

$$P_{\perp} = (I_{\text{up}}^+ - I_{\text{down}}^+ + I_{\text{up}}^- - I_{\text{down}}^-) / I_0 \quad (5)$$

averages out the effect of the light helicity and therefore captures the contribution arising due to final-state interference. As mentioned above, in our case of a centrosymmetric crystal and excluding interface effects, the initial state spin polarization vanishes. Since the $y - z$ plane coincides with a crystal mirror plane, the y -component of the spin polarization and the circular polarization simultaneously change sign upon mirroring the experiment at the $y - z$ plane. Therefore, this symmetry dictates that $P(k_x) = -P(-k_x)$. Neglecting the linear dichroism, which is suppressed to a large extent by the normalization to I_0 , one also obtains $P(k_y) = P(-k_y)$ because the $x - z$ plane also coincides with a crystal mirror plane.

- (iii) The spin polarization P_{OO} caused by optical orientation (figure 4(b)) is defined as

$$P_{OO} = (I_{\text{up}}^- - I_{\text{down}}^- - I_{\text{up}}^+ + I_{\text{down}}^+) / I_0. \quad (6)$$

In this linear combination P_{\perp} (equation (5)) is averaged out and one detects exclusively the effect from optical spin orientation. The symmetry consideration leads to the conditions $P(k_x) = P(-k_x)$ and $P(k_y) = P(-k_y)$. The optical orientation is a matrix-element effect governed by Clebsch–Gordan coefficients. According to the relativistic selection rules, the sign of the spin polarization

reflects the double-group symmetry of the initial state ([7] and references therein).

- (iv) The circular dichroism texture (figure 3(c))

$$A_{CDAD} = (I_{\text{up}}^- + I_{\text{down}}^- - I_{\text{up}}^+ - I_{\text{down}}^+) / I_0 \quad (7)$$

measures the change of the spin-integrated intensity upon reversal of the light helicity. The symmetry consideration of the present experiment results in $A(k_x) = -A(-k_x)$ and $A(k_y) = A(-k_y)$; i.e. similar to case (ii). However, its physical origin is very different and can be understood from phase-dependent overlap integrals of initial and final states as described in [41].

Using equation (5), we determine P_{\perp} . The result shown in figure 4(a) reveals a rich fine structure that results from the final-state wavelength (1.68 \AA) being smaller than the nearest-neighbour distance (1.81 \AA) and from the fact that this component results from the spin-dependent interference of outgoing partial waves.

The optical spin orientation P_{OO} (equation (6)) depicted in figure 4(b) also reveals a high spin polarization with distinctly different symmetry behaviour than P_{\perp} . We note that this result is equivalent to the case of the GaAs-based spin-polarized electron source but using excitation at much higher photon energy.

Figure 4(c) finally depicts the circular dichroism in the angular distribution A_{CDAD} measured at the high-energy working point of the spin filter. From an atomic-like perspective, A_{CDAD} is determined by the interference of different outgoing partial waves being sensitive to their phase-shift differences. As a consequence of its different origin, A_{CDAD} significantly differs from P_{\perp} , although both have the same symmetry properties.

Testing the validity of equation (1) on our data, we depict values for PI defined in figure 5(a) along the profile lines shown in figure 4, corresponding to the difference of intensity instead of spin polarization values. We have chosen this data representation to avoid large data scattering at positions where the intensity almost vanishes. We find that the positive P_{\perp} maximum at $k_x = 0.25 \text{ \AA}^{-1}$ on profile 1 coincides with negative values for P_{OO} and A_{CDAD} . On profile 2 P_{\perp} changes sign at $k_x = 0.25 \text{ \AA}^{-1}$ from minus to plus, while P_{OO} changes sign from plus to minus. Both sign changes coincide with

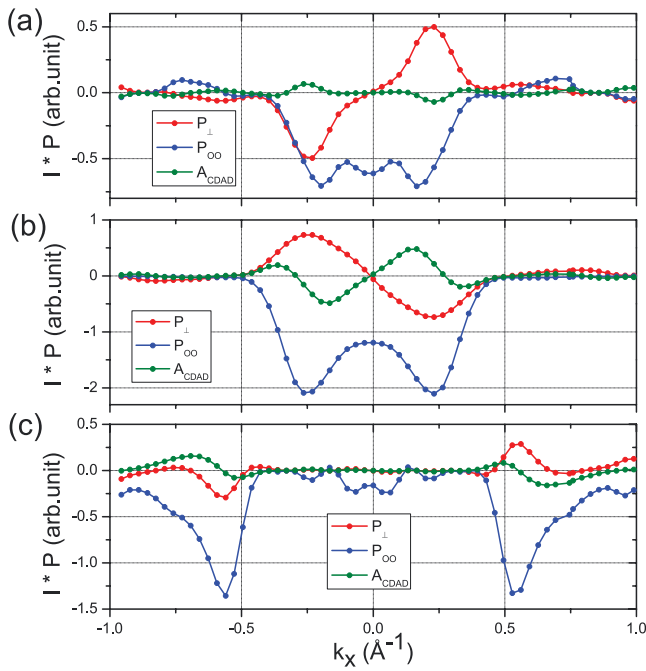


Figure 5. (a) $P_{\perp}I$, $P_{OO}I$, and $A_{CDAD}I$ along line 1 in figures 4(a) and (b) same for line 2 and (c) same for line 3. The P_iI values are scaled so that a value of 1.4 at the extrema correspond to a complete spin polarization.

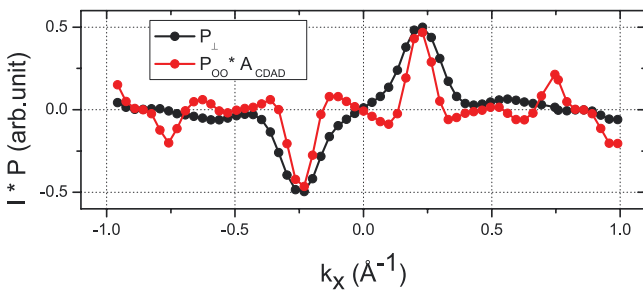


Figure 6. $P_{\perp}I$ and product of $P_{OO}I$ and A_{CDAD} along line 1 in figure 4(a).

a negative maximum for A_{CDAD} . The positive P_{\perp} extrema near $k_x = 0.6 \text{ \AA}^{-1}$ on profile 3 coincides with $P_{OO} < 0$ and $A_{CDAD} < 0$ in this region. These observations confirm relation (1).

For a quantitative comparison figure 6 shows the product $P_{OO}I \times A_{CDAD}$ in direct comparison to $P_{\perp}I$, revealing a fairly good agreement. The remaining discrepancies can partly originate from the modification of equation (1) by the spin-orbit interaction. Moreover, the larger statistical variation of P_{\perp} required a Gaussian averaging as compared to A_{CDAD} . The gross features are well described by equation (1).

Conclusion

In conclusion, by using the Feynman formalism, we derive a relation between the circular dichroism in the angular distribution, the spin polarization caused by optical orientation with circularly polarized light, and the spin polarization due to spin-orbit scattering, which holds for photoemission from

spin-degenerate initial states. To confirm this relation, we measure the spin polarization of photoelectrons emitted by soft x-rays from initial tungsten bulk states at the Fermi level. Spin polarization originating from optical spin orientation by circularly polarized x-rays (Fano component) and a contribution from spin-orbit scattering resulting from interference of final-state partial waves (Mott component P_{\perp}) are distinguished by means of four independent measurements. P_{\perp} arises even for unpolarized or linearly polarized light. The spin polarization is disentangled from the circular dichroism of the photoelectron intensity (CDAD). In particular, CDAD shows a texture different from the spin polarization P_{\perp} , although the symmetry conditions for both quantities are identical.

A spin polarization that does not result from optical orientation has previously been considered to involve either an interface breaking the inversion symmetry or a crystal without inversion symmetry [42]. Therefore, the observed component P_{\perp} from initial spin degenerate bulk states represents an interesting phenomenon. The demonstration of spin polarization of electrons excited in the soft x-ray regime, previously considered as an extremely time-consuming experiment, also paves the way to the analysis of the spin-polarization texture for initial bulk states in non-inversion symmetric crystals or ferromagnets, where the spin polarization resulting from the initial state polarization adds up to the effects described in this article.

Acknowledgments

We thank the team of PETRA beamline P04 for excellent support. Funding by BMBF (project 05K16UMC) and by the German Research Foundation (DFG) Collaborative Research Centre SFB/TRR173 ‘Spin + X’.

ORCID iDs

Dmitry Vasilyev  <https://orcid.org/0000-0003-2870-3851>

References

- [1] Kessler J 1976 *Polarized Electrons* (Berlin: Springer)
- [2] Kirschner J 1985 *Polarized Electrons at Surfaces* (Berlin: Springer)
- [3] Feder R 1985 *Polarized Electrons in Surface Physics* (Singapore: World Scientific)
- [4] Bänninger U, Busch G, Campagna M and Siegmann H C 1970 *Phys. Rev. Lett.* **25** 585
- [5] Pierce D and Meier F 1976 *Phys. Rev. B* **13** 5484
- [6] Kisker E, Schröder K, Campagna M and Gudat W 1984 *Phys. Rev. Lett.* **52** 2285
- [7] Eyers A, Schäfers F, Schönhense G, Heinzmann U, Oepen H P, Hünlich K, Kirschner J and Borstel G 1984 *Phys. Rev. Lett.* **52** 1559
- [8] Schönhense G, Eyers A and Heinzmann U 1986 *Phys. Rev. Lett.* **56** 512
- [9] Hsieh D, Qian D, Wray L, Xia Y, Hor Y S, Cava R J and Hasan M Z 2008 *Nature* **442** 970
- [10] Xu S Y *et al* 2015 *Nat. Phys.* **11** 748

- [11] Bradlyn B, Elcoro L, Cano J, Vergniory M G, Wang Z, Felser C, Aroyo M I and Bernevig B A 2017 *Nature* **547** 298
- [12] Roth C, Hillebrecht F U, Park W G, Rose H B and Kisker E 1994 *Phys. Rev. Lett.* **73** 1963
- [13] Klebanoff L E, Campen D G V and Pouliot R J 1994 *Phys. Rev. B* **49** 2047
- [14] Johnson P D 1997 *Rep. Prog. Phys.* **60** 1217
- [15] Stryganyuk G et al 2012 *Japan. J. Appl. Phys.* **51** 016602
- [16] Ueda S, Mizuguchi M, Kojima T, Ishimaru S, Tsujikawa M, Shirai M and Takanashi K 2014 *Appl. Phys. Lett.* **104** 132402
- [17] Gloskowskii A et al 2012 *J. Electron Spectrosc. Relat. Phenom.* **185** 47
- [18] Kozina X, Ikenaga E, Barbosa C E V, Ouardi S, Karel J, Yamamoto M, Kobayashi K, Elmers H J, Schönhense G and Felser C 2016 *J. Electron Spectrosc. Relat. Phenom.* **211** 12
- [19] Gray A X et al 2011 *Nat. Mater.* **10** 759
- [20] Medjanik K et al 2017 *Nat. Mater.* **16** 615
- [21] Kolbe M, Lushchik P, Petereit B, Elmers H J, Schönhense G, Oelsner A, Tusche C and Kirschner J 2011 *Phys. Rev. Lett.* **107** 207601
- [22] Tusche C, Ellguth M, Ünal A A, Chiang C T, Winkelmann A, Krasnyuk A, Hahn M, Schönhense G and Kirschner J 2012 *Appl. Phys. Lett.* **108** 066808
- [23] Henk J, Scheunemann T, Halilov S V and Feder R 1996 *J. Phys.: Condens. Matter* **8** 47
- [24] Miyamoto K, Kimura A, Kuroda K, Okuda T, Shimada K, Namatame H, Taniguchi M and Donath M 2011 *Appl. Phys. Lett.* **99** 032505
- [25] Kirschner J, Feder R and Wendelken J 1981 *Phys. Rev. Lett.* **47** 614
- [26] Fano U 1969 *Phys. Rev.* **178** 131
- [27] Heinzmann U and Dil J H 2012 *J. Phys.: Condens. Matter* **24** 173001
- [28] Heinzmann U, Schönhense G and Kessler J 1979 *Phys. Rev. Lett.* **42** 1603
- [29] Schönhense G 1980 *Phys. Rev. Lett.* **44** 640
- [30] Fedchenko O et al 2019 *New J. Phys.* **21** 013017
- [31] Schönhense G et al 2017 *Ultramicroscopy* **183** 19
- [32] Schönhense G, Medjanik K and Elmers H 2015 *J. Electron Spectrosc. Relat. Phenom.* **200** 94
- [33] Vasilyev D, Tusche C, Giebels F, Gollisch H, Feder R and Kirschner J 2015 *J. Electron Spectrosc. Relat. Phenom.* **199** 10
- [34] Abrikosov A, Gorkov L and Dzyaloshinsky I 1975 *Methods of Quantum Field Theory in Statistical Physics* (New York: Dover)
- [35] Baker U and Shirley D A 1996 *VUV and Soft X-Ray Photoionization* (New York: Springer) pp 1–45
- [36] Eminyan M and Lampel G 1980 *Phys. Rev. Lett.* **45** 1171
- [37] Schönhense G 1990 *Phys. Scr.* **T31** 255
- [38] Kessler J 1981 *Commun. At. Mol. Phys.* **10** 47
- [39] Heinzmann U 1980 *J. Phys. B* **13** 4367
- [40] Wang Y H, Hsieh D, Pilon D, Fu L, Gardner D R, Lee Y S and Gedik N 2011 *Phys. Rev. Lett.* **107** 207602
- [41] Cherepkov N 1982 *Chem. Phys. Lett.* **87** 344
- [42] Krempaský J et al 2016 *Nat. Commun.* **7** 13071